



**The Abdus Salam
International Centre for Theoretical Physics**



2218-3

Mediterranean School on Nano-Physics
held in Marrakech - MOROCCO

2 - 11 December 2010

Comparison of Topographic Correction Methods

Presented by: STANKEVICH Sergey
(RICHTER R., Kellenberger T and Kaufmann H.)
National Academy of Science of Ukraine
CASRE Aerospace Research Center of the Earth
55B Oles Gonchar Str. 01601
Kiev
UKRAINE

Article

Comparison of Topographic Correction Methods

Rudolf Richter ^{1,*}, Tobias Kellenberger ² and Hermann Kaufmann ³

¹ DLR – German Aerospace Center, D-82234 Wessling, Germany

² Federal Office of Topography swisstopo, Seftigenstr. 264, CH-3084 Wabern, Switzerland;
E-Mail: tobias.kellenberger@swisstopo.ch

³ GFZ – GeoResearchCenter Potsdam, Telegraphenberg, D-14473 Potsdam, Germany;
E-Mail: charly@gfz-potsdam.de

* Author to whom correspondence should be addressed; E-Mail: rudolf.richter@dlr.de;
Tel.: +49-8153 281 160; Fax: +49-8153 281 458

Received: 8 June 2009; in revised form: 30 June 2009 / Accepted: 3 July 2009 /

Published: 6 July 2009

Abstract: A comparison of topographic correction methods is conducted for Landsat-5 TM, Landsat-7 ETM+, and SPOT-5 imagery from different geographic areas and seasons. Three successful and known methods are compared: the semi-empirical C correction, the Gamma correction depending on the incidence and exitance angles, and a modified Minnaert approach. In the majority of cases the modified Minnaert approach performed best, but no method is superior in all cases.

Keywords: topography; C, Gamma, and modified Minnaert methods; multi-sensor imagery

1. Introduction

In mountainous areas there is a strong influence of the topography on the signal recorded by spaceborne optical sensors, i.e., for the same surface cover slopes oriented away from and towards the sun will appear darker and brighter, respectively, if compared to a horizontal geometry. This behaviour causes problems for a subsequent scene classification and thematic evaluation. Therefore, different topographic correction methods were developed to eliminate or at least reduce the topographic influence [1-9]. The contribution of Riano *et al.* [6] summarizes the most frequently used topographic

normalization methods. It ranks the modified C method first, based on the evaluation of a mapping of vegetation types in Landsat TM data from an area in the Toledo mountains, Spain. The modification concerned an averaging of the DEM slopes over 5×5 pixels, but most other contributions work with non-smoothed slope values [3-5]. Some authors employ the Lambert normalization [4,8,9], others include the sensor view geometry in addition to the solar illumination.

While each paper yields good results for the respective investigated scene, a comparison of the methods for different areas (vegetated, arid, semi-arid) and different sensors is missing, but would be of great interest. A comprehensive study for different sensors, geographical regions, and seasons is a huge effort outside the scope of a single paper. However, this study is a first step into this direction, as it comprises an evaluation of data from three different sensors (SPOT-5, Landsat-5 TM, and Landsat-7 ETM+), two different geographic areas (Switzerland and Israel), and some multi-temporal (SPOT-5, Switzerland) data. The investigation contains a comparison of three known often-employed topographic correction approaches, the C method, the Gamma method that includes the viewing geometry in addition to the solar illumination geometry, and a modified Minnaert technique.

2. Methods

A brief survey of the methods is summarized here. All proposed methods rely on a digital elevation model (DEM) of the scene to describe the topography. If θ_n , θ_s , ϕ_s , ϕ_n denote solar zenith angle, terrain slope, solar azimuth, and topographic azimuth, respectively, the local solar illumination angle β can be obtained from the topographic slope and aspect angles and the solar geometry:

$$\cos \beta(x, y) = \cos \theta_s \cos \theta_n(x, y) + \sin \theta_s \sin \theta_n \cos \{ \phi_s - \phi_n(x, y) \} \quad (1)$$

where x , y indicate the pixel coordinates in an image that depend on the terrain slope θ_n and aspect ϕ_n . If ρ_T and ρ_H denote the reflectance of an inclined (terrain) and a horizontal surface, respectively, then the Lambertian method of topographic normalization is defined as:

$$\rho_H = \rho_T \frac{\cos \theta_s}{\cos \beta} \quad (2)$$

For a low illumination, i.e., small values of $\cos \beta$, the corrected reflectance is too large and the corresponding parts of an image are overcorrected. All methods can be applied to surface reflectance (after atmospheric correction) or the apparent or top-of-atmosphere (TOA) reflectance, i.e., $\rho = \pi L / E \cos \theta_s$ (L = at-sensor radiance, E = extraterrestrial solar irradiance). The Minnaert normalization [6,10] is defined as:

$$\rho_H = \rho_T \left(\frac{\cos \theta_s}{\cos \beta} \right)^K \quad (3)$$

where the exponent K usually ranges between 0 and 1. If $\cos \beta$ tends to 0, the method encounters similar problems as the Lambertian approach of Equation (2).

Similar to the Minnaert approach, our first method the C normalization belongs to a class of non-Lambertian methods [6]. It can be defined as:

$$\rho_H = \rho_T \frac{\cos \theta_s + c_k}{\cos \beta + c_k} \quad (4)$$

where k indicates the channel dependence, and $\rho_T = a_k + b_k \cos\beta$, and a_k, b_k are calculated from the regression equation of the terrain reflectance versus the local illumination angle ($c_k = b_k/a_k$). This approach avoids the problems associated with small values of $\cos\beta$ by adding the term c_k in the denominator. The c_k accounts for the diffuse radiance component if TOA reflectance data is used, and for residual effects in case of surface reflectance.

The second approach [7], called ‘‘Gamma’’ here, calculates the horizontal reflectance as a function of the solar and terrain angles (θ_s, β) and also depends on the sensor view angles on a flat terrain (θ_v) and the inclined terrain (β_v):

$$\rho_H = \rho_T \gamma = \rho_T \frac{\cos \theta_s + \cos \theta_v}{\cos \beta + \cos \beta_v} \quad (5)$$

It is an extension of Equation (2) and avoids an overcorrection in faintly illuminated areas with the additive term $\cos \beta_v$ in the denominator.

The third method is described in detail in references [5,11]. Basically, it is a modified Minnaert approach, but with a set of empirical rules that were successfully tested on many rugged terrain scenes. As a first step, the surface reflectance is computed based on a Lambertian reflectance law ρ_L . Then if the local solar illumination angle β exceeds a threshold β_T (i.e., in areas of low illumination where ρ_L might become high), the updated surface reflectance is reduced according to:

$$\rho_{MM} = \rho_L \left(\frac{\cos \beta}{\cos \beta_T} \right)^b \quad (6)$$

The index ‘MM’ stands for modified Minnaert. If the local illumination angle does not exceed the threshold β_T , then Equation (6) is not applied and the Lambertian reflectance is retained ($\rho_{MM} = \rho_L$). The following set of empirical rules is used in combination with Equation (6), see reference [11]:

- The threshold angle is set as $\beta_T = \theta_s + 20^\circ$, i.e., 20° above the solar zenith angle, if $\theta_s < 45^\circ$.
- If $45^\circ \leq \theta_s \leq 55^\circ$ then $\beta_T = \theta_s + 15^\circ$.
- If $\theta_s > 55^\circ$ then $\beta_T = \theta_s + 10^\circ$, i.e., a higher solar zenith angle requires a threshold closer to the solar zenith, because the correction must take place earlier.
- Exponent $b = 1/2$ for non-vegetation.
- Exponent $b = 3/4$ for vegetation in the visible spectrum ($\lambda < 720 \text{ nm}$).
- Exponent $b = 1/3$ for vegetation if $\lambda \geq 720 \text{ nm}$.

In addition, if the correction factor $(\cos\beta / \cos\beta_T)^b$ is smaller than 0.25 (i.e., local solar zenith angle much higher than the threshold angle) it will be reset to 0.25 to prevent a too strong reduction.

In this study, the C normalization is applied to TOA reflectance images, and the other candidates (Gamma and modified Minnaert MM) are evaluated based on surface reflectance data [4,5,7,8], i.e., with a combined atmospheric / topographic correction. The reason for using the TOA reflectance with the C method here is that it is much easier to use (no atmospheric correction necessary) and it is the most frequently used method in practice. However, our ranking of the C method is independent of applying it to TOA or surface reflectance. On the other hand, the Gamma and MM techniques are always applied to surface reflectance data in the literature.

3. Results and Discussion

Following the suggestion of some authors [1,6,7] the quality of the topographic correction can be estimated by the reduction of the standard deviation of the reflectance within each surface cover class. We use the coefficient of variation (CV in percent) as a metric which is defined as:

$$CV = 100 \sigma / mean \quad (7)$$

where σ and *mean* are the standard deviation and mean class reflectance values, respectively. A coarse classification of each scene is conducted based on the MM product (i.e., after atmospheric / topographic correction) employing three classes. Class 1 is dark vegetation (coniferous forest), class 2 consists of deciduous and mixed forests as well as agricultural fields, and class 3 is non-vegetation, see [11,12] for details on the classification algorithm. The second quality measure is the visual appearance of processed images as the human observer is critical and sensitive to topographically related artifacts. Table 1 summarizes the locations, acquisition dates, and geometries for the six scenes investigated here. The SPOT-5 scenes are taken from a project to generate a SPOT-5 mosaic of Switzerland. The Landsat-7 ETM+ scene also covers part of Switzerland, whereas the Landsat-5 TM scene was recorded over Makhtesh Ramon, Israel. For the nadir-viewing Landsat scenes the view azimuth angle is not defined. The SPOT scenes have different view or tilt angles, from near-nadir to 26.8° off-nadir. A positive view angle indicates a tilt right (west) with respect to the platform movement, a negative angle left (east).

Table 1. List of scenes (SZA = solar zenith angle, SAA = solar azimuth angle, VZA = view zenith angle, VAA = view azimuth angle).

ID	Sensor	Acquisition Date	SZA / SAA	VZA / VAA
(a)	SPOT-5	2004-05-29	25.1° / 164.9°	26.8° / 289.1°
(b)	SPOT-5	2005-07-20	27.5° / 154.0°	13.2° / 287.0°
(c)	SPOT-5	2005-09-06	42.6° / 155.5°	-15.7° / 103.3°
(d)	SPOT-5	2005-09-21	46.7° / 163.7°	2.3° / 285.6°
(e)	L7 ETM+	1999-09-11	45.8° / 153.3°	0° / -
(f)	L5 TM	1995-09-12	44.5° / 124.8°	0° / -

The topographic measures for the SPOT scenes are based on a 10 m resolution bilinear resampling of the original 25 m DEM during the orthorectification. Terrain measures for the Landsat scenes are also determined from a 25 m DEM, but are scaled to 30 m. Figures 1 to 6 show the results of processing for the six scenes, and Figure 7 presents the coefficient of variation (CV) evaluation for each reflective spectral band. For the visual assessment, smaller sub-scenes are always displayed in critical areas with large variations of the topography.

3.1. Scene (a)

Figure 1 displays a sub-scene of the SPOT-5 scene (a). It has the largest off-nadir viewing angle (26.8°) of all considered scenes. Elevations range between 300 m and 1700 m, slopes between 0° and 42°. The illumination map ($\cos\beta$) represents the cosine of the local solar zenith angle and incorporates the topography. Bright areas receive a high illumination, dark areas are the critical ones, representing steep

slopes oriented away from the sun. Therefore, the methods will likely yield different results in those dark areas. This can indeed be observed when comparing Figure 1 (d) to (f). From the visual impression the MM method ranks first, followed by the C correction, Gamma ranks last, because of the large yellow areas in faintly illuminated regions. In the false colour image, the second rank of the C approach is not very clear, but the better performance of MM is obvious from the results of the first band, compare Figure 1 (g) with (i). The classification map (Figure 1 (c)) presents class1 (coniferous, coded as dark green), and class 2 (deciduous and agricultural, coded medium green). A comparison of Figure 1 (b) and Figure 1 (c) shows that the classification is only marginally dependent on the illumination.

Figure 1. Sub-scene of (a), RGB = bands 4, 3, 2 (1650, 840, 660 nm). (a) Original. (b) Illumination. (c) Classification map. (d) C correction. (e) Gamma correction. (f) MM correction, (g) C (band 1). (h) Gamma (band 1). (i) MM (band 1).

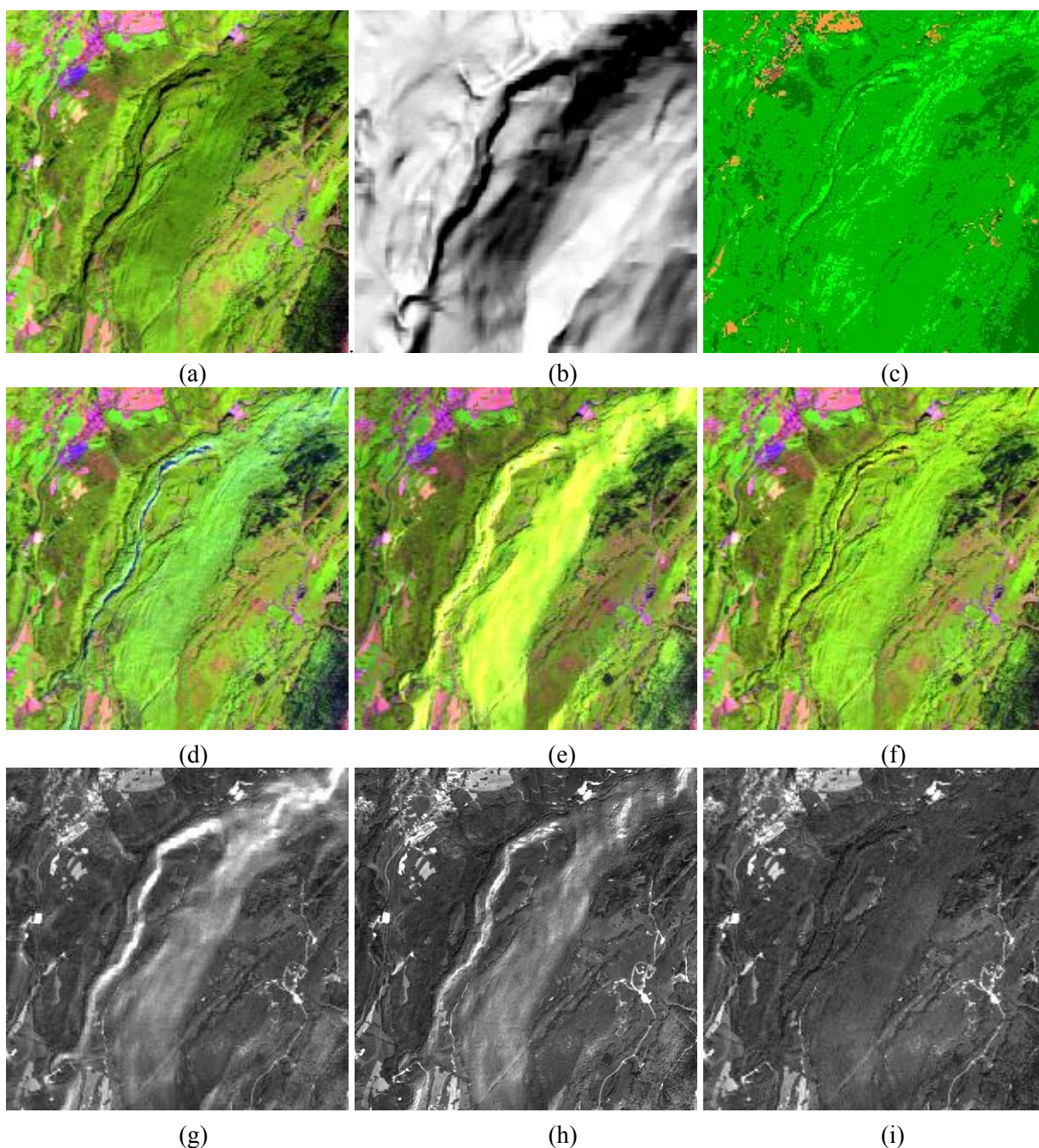
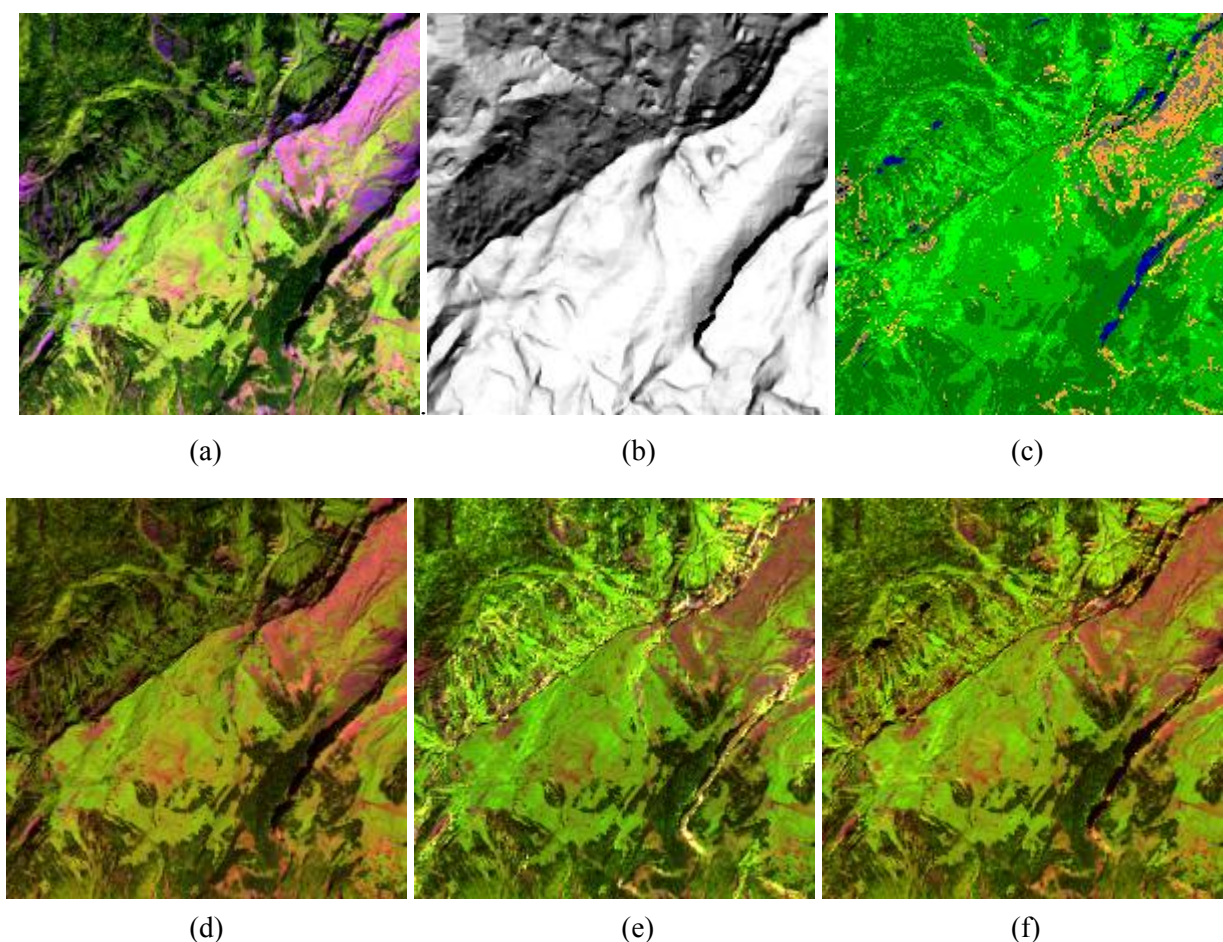


Figure 7 (a) presents the CV values for the classes 1 and 2. The average slope values are 19° (class 1) and 22° (class 2), not counting pixels in the flat plane. As low values indicate the best elimination of topographic features, the C method ranks first for the visible bands (1, 2), while C and MM achieve the same quality for the NIR and SWIR bands (3, 4). However, the visual comparison of Figure 1 (g),(i) clearly indicates a better performance of the MM algorithm.

3.2. Scene (b)

Figure 2 displays a sub-scene of the SPOT-5 scene (b). It has a medium off-nadir viewing angle (13.2°). Elevations range between 600 m and 3,600 m, slopes between 0° and 64° . From the visual impression the MM method ranks first, followed by the Gamma, then the C algorithm. The Gamma image contains artifacts (yellow pixels) which do not appear in the MM corrected scene. Figure 7 (b) presents the CV values for class 1. Results for class 2 show a similar trend, therefore, they are not included. The average slope of the terrain is 32° , not counting pixels in the flat plane, which is rather high. Again, for the visible bands (1, 2) the C method (+ symbol) ranks first, followed by MM, and Gamma. For the NIR, SWIR bands the ranking is MM, C, Gamma. However, the visual inspection places MM first for all bands.

Figure 2. Sub-scene of (b), RGB = bands 4, 3, 2 (1650, 840, 660 nm). (a) Original. (b) Illumination. (c) Classification map. (d) C correction. (e) Gamma. (f) MM correction.

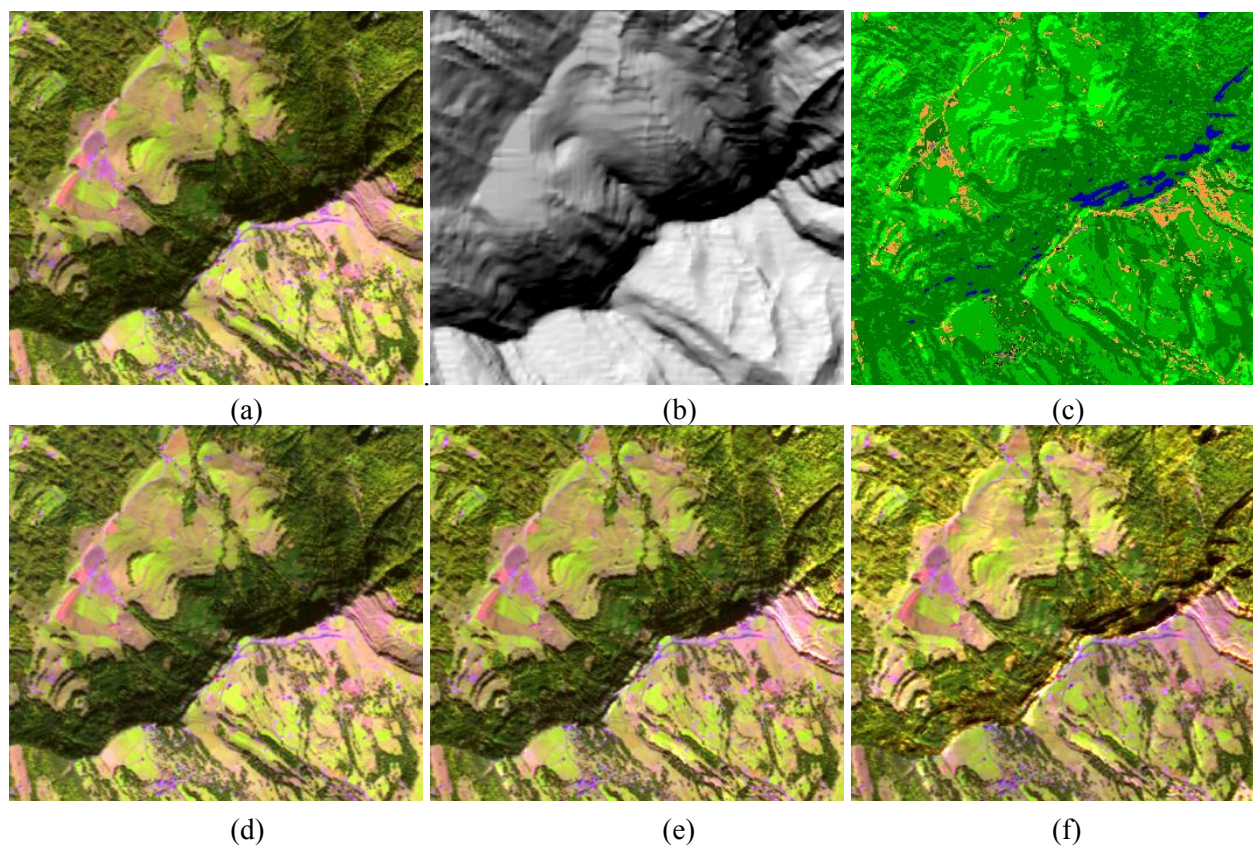


3.3. Scene (c)

Figure 3 displays a sub-scene of the SPOT-5 scene (c). It has a medium off-nadir viewing angle (15.7°). Elevations range from 400 m to 1900 m, and steep slopes up to 50° can be found. A comparison of the illumination (Figure 3b) and classification maps (Figure 3c) shows no correlation of class assignment and terrain illumination except for some blue areas (topographic shadow, misclassified as water) that do not belong to the evaluated classes 1 (dark green) and 2 (medium green). From the visual impression the MM method ranks first, followed by the Gamma, then the C algorithm.

Figure 7 (c) presents the CV values for class 1. Results for class 2 show a similar trend, therefore, they are not included. The average slope of the terrain is 26° . Again, for the visible bands (1, 2) the C method (+ symbol) ranks first, followed by MM, and Gamma. For the NIR, SWIR bands the ranking is MM, C, Gamma. However, the visual inspection places MM first for all bands.

Figure 3. Sub-scene of (c), RGB = bands 4, 3, 2 (1650, 840, 660 nm). (a) Original. (b) Illumination. (c) Classification. (d) C correction. (e) Gamma correction. (f) MM correction.

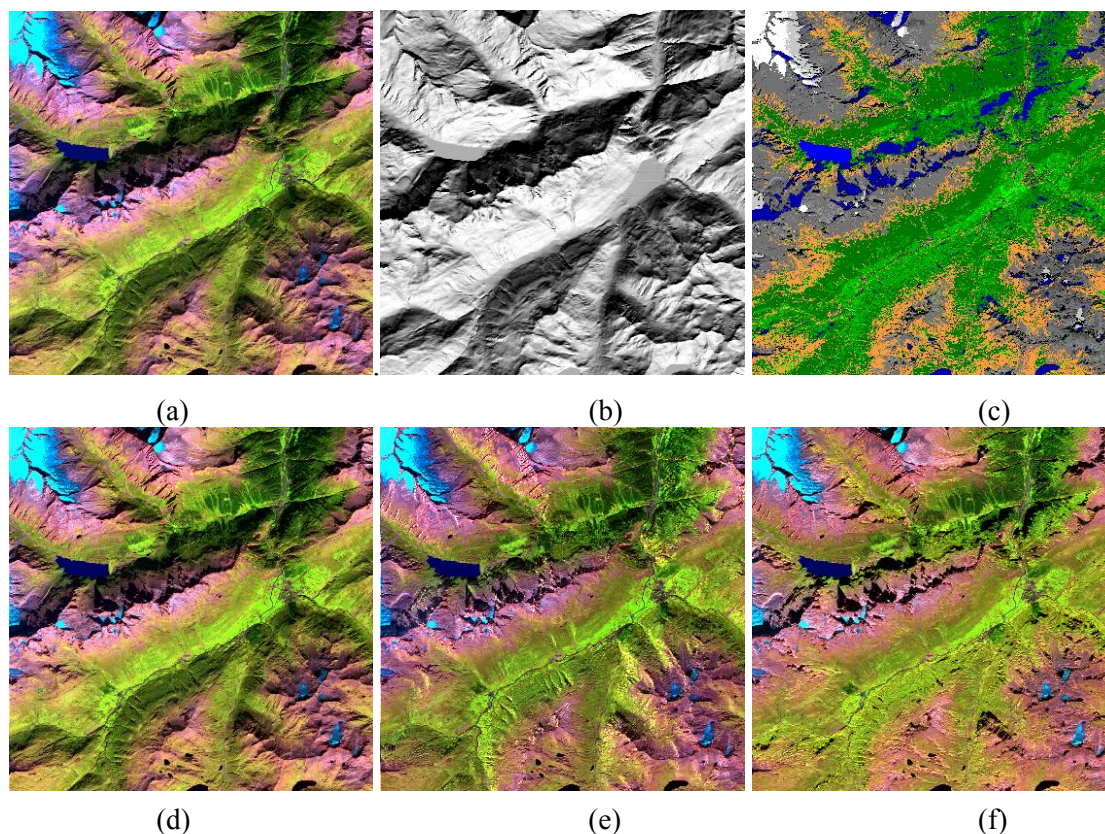


3.4. Scene (d)

Figure 4 displays a sub-scene of the SPOT-5 scene (d). It has a near-nadir viewing angle (2.3°). Elevations range between 1,200 m and 3,000 m, and steep slopes up to 58° . In the classification map of Figure 4c some misclassifications occur in regions where the illumination is 0 (topographic shadow), see the blue areas indicating water bodies. However, these pixels are not used in the evaluation, and the vegetation classes 1 and 2 are correctly assigned. From the visual impression the MM method again ranks first, followed by the Gamma, then the C algorithm.

Figure 7 (d) presents the CV values for class 1. Results for class 2 show a similar trend, therefore, they are not included. The average slope of the terrain is 21° , not considering the flat terrain. Again, for the visible bands (1, 2) the C method ranks first, MM and Gamma values are nearly the same. For the NIR, SWIR bands the ranking is MM, Gamma, C. However, the visual inspection clearly places MM first for all bands.

Figure 4. Sub-scene of (d), RGB = bands 4, 3, 2 (1650, 840, 660 nm). (a) Original. (b) Illumination. (c) Classification. (d) C correction. (e) Gamma correction. (f) MM correction.



3.5. Scene (e)

Figures 5 (a) and 5 (b) display two different sub-scenes of the Landsat-7 ETM+ scene (e). The scene was orthorectified with a Swisstopo 25 m DEM scaled to 30 m. Elevations range between 400 m and 1,100 m, slopes reach values up to 34° . The reason for selecting two sub-scenes is to demonstrate that the best performance ranking can even change from one sub-scene to the next within the same large scene. In the true colour image of Figure 5a, the visual impression indicates that the best performance in suppressing topographic features is achieved with the C method, followed by MM, and Gamma. However, in the second sub-scene of Figure 5 (b) with the NIR and SWIR bands the ranking is MM, followed by Gamma, then the C algorithm, while the true colour image (not shown for space reasons) yields the ranking MM, C, Gamma.

Figure 7 (e) presents the CV values for classes 1 and 2. The C method ranks first for the visible bands (1, 2, 3) while MM is superior for the NIR and SWIR bands. CV values for class 1 (conifers) are higher than for class 2 (deciduous forests, agricultural fields), because the mean reflectance values are lower for

class 1, especially in the NIR and SWIR region, i.e., for the same standard deviation σ the $CV = 100 \sigma / mean$ will be larger.

Figure 5a. Sub-scene 1 of (e), RGB = bands 3, 2, 1 at 660, 560, 480 nm. (a) Original. (b) Illumination. (c) Classification. (d) C correction. (e) Gamma correction. (f) MM correction.

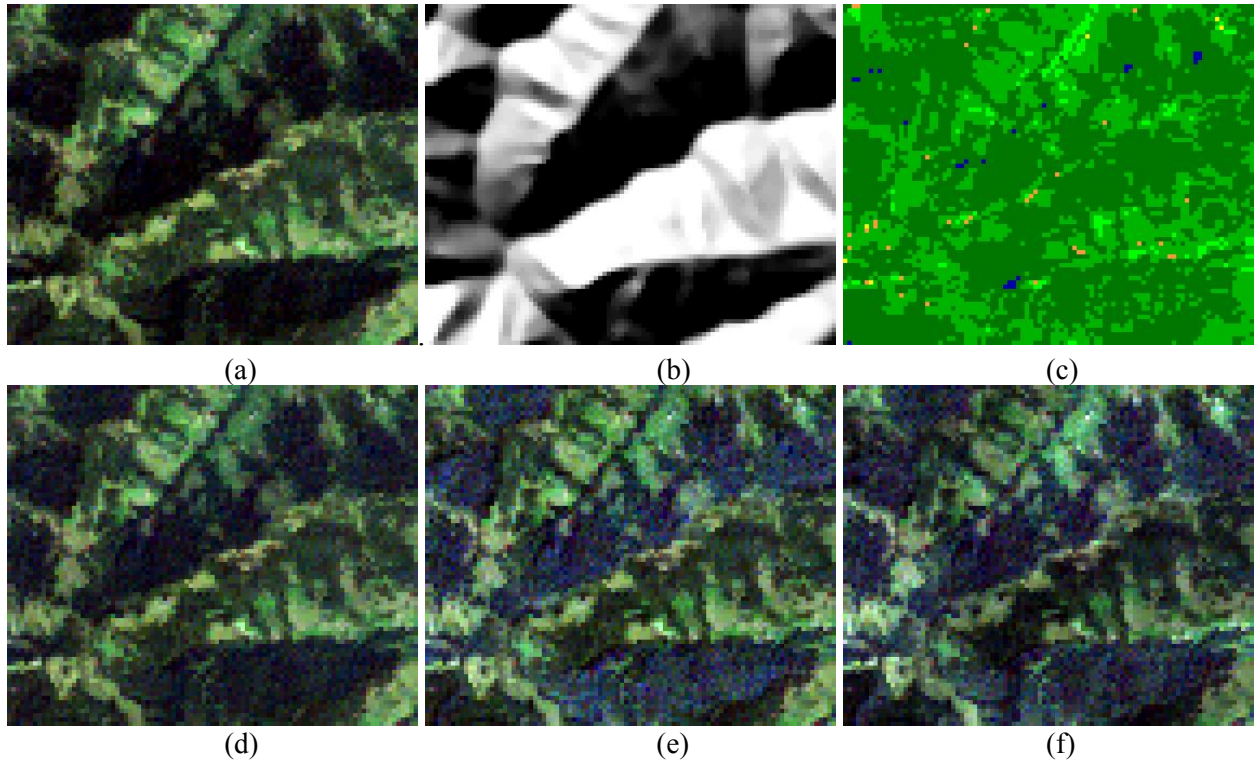
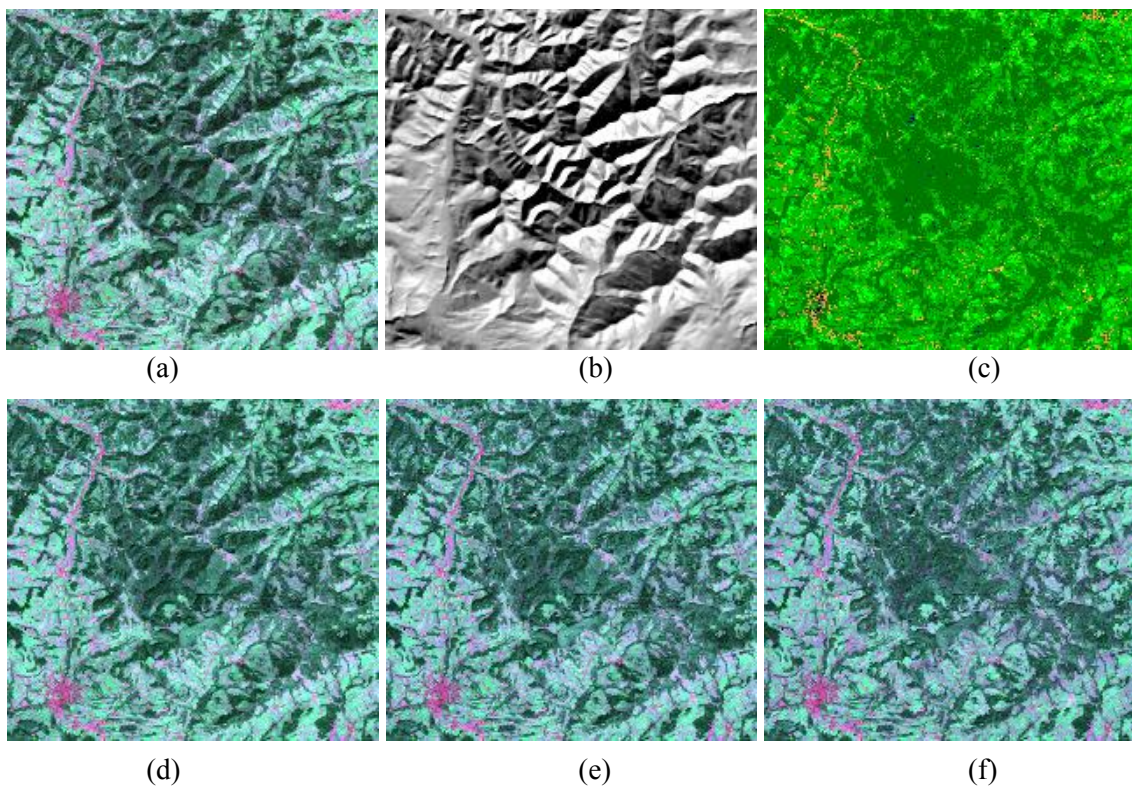


Figure 5b. Sub-scene 2 of (e), RGB = bands 7, 4, 5 (2200, 840, 1600 nm). (a) Original. (b) Illumination. (c) Classification. (d) C correction. (e) Gamma correction. (f) MM correction.



3.6. Scene (f)

Figure 6 shows a sub-scene of Landsat-5 TM from the Makhtesh Ramon area in Israel. The scene was orthorectified with a 25 m DEM scaled to 30 m. Elevations range between 200 m and 800 m, slope values reach 31° . The classification map is not shown as it contains only the sand class and no vegetation. Two locations have been marked in the image: the center of the square symbol shows pixels oriented to the sun [bright in Figure 6 (b)], and the center of the circle indicates pixels oriented away from the sun [dark in Figure 6 (b)]. From the visual impression, the best performance in eliminating topographic features is achieved with the MM algorithm, followed by Gamma, then the C method. Although only one RGB band combination is shown here for space reasons, this statement holds true for all band combinations.

Figure 6. Sub-scene of (f), RGB = bands 7, 4, 1 (2200, 840, 480 nm). (a) Original. (b) Illumination. (c) C correction. (d) Gamma correction. (e) MM correction.

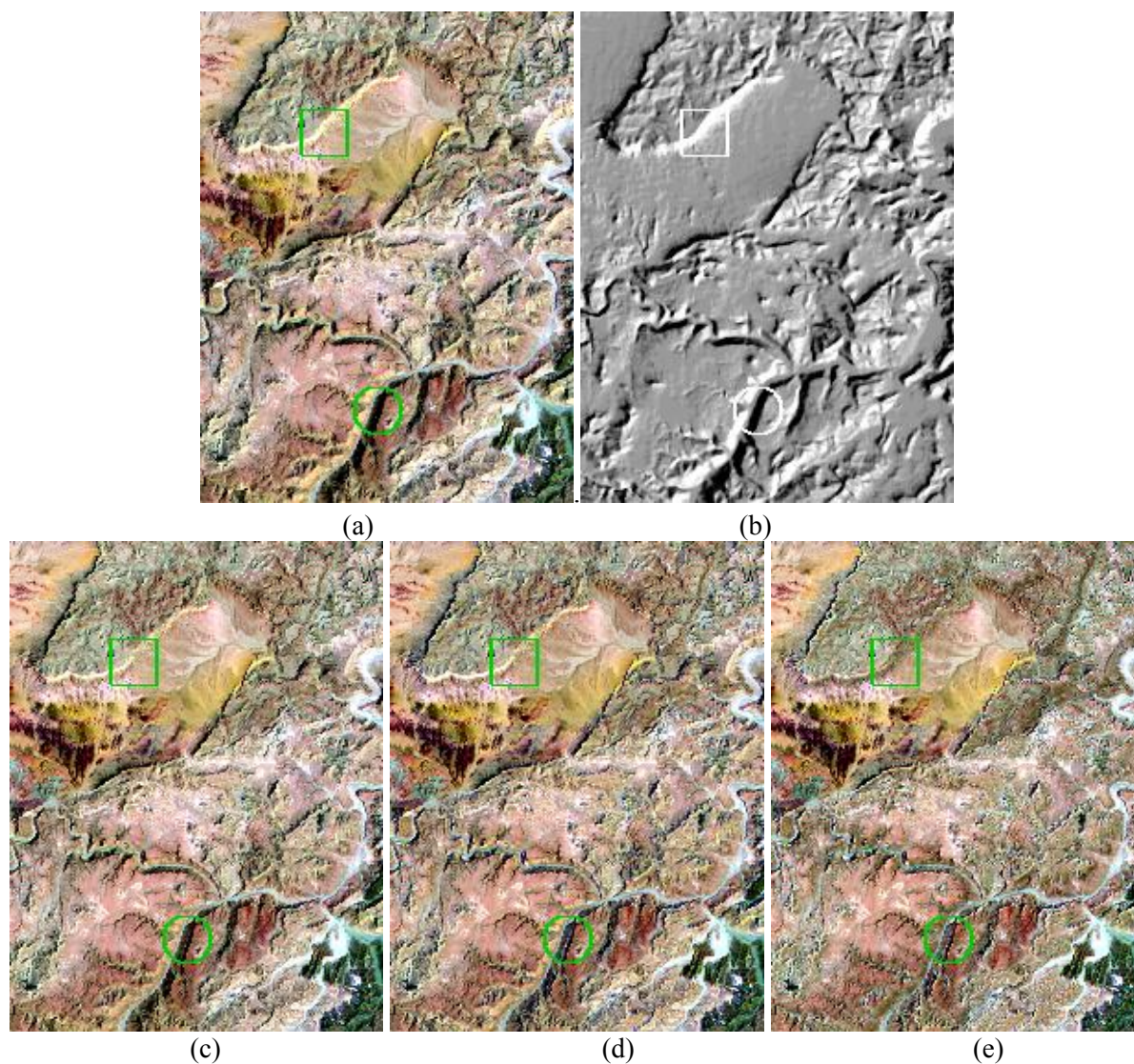
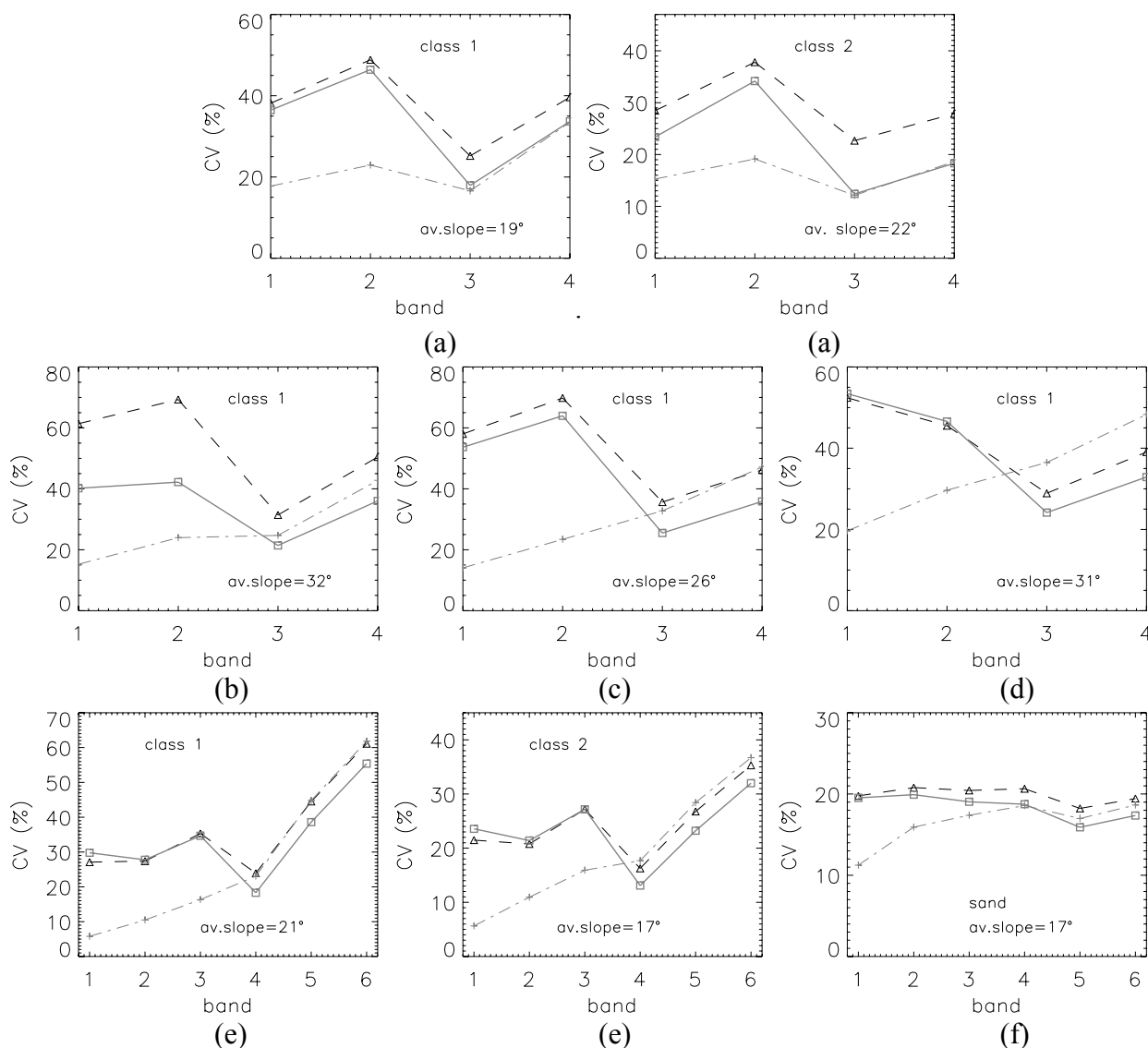


Figure 7 (f) presents the CV values for the six reflective bands of TM. For the selected arid region, there exist only class 3 pixels (sand). Similar to the previous results with the SPOT-5 and ETM+ scenes,

the C method has the best performance in the visible bands. The MM algorithm again ranks first in the NIR and SWIR bands. In Figure 7, for scenes (b), (c), (d) results are only shown for class 1 because those for class 2 are very similar. Scene (f) has no vegetation, so only class 3 (sand) is displayed.

Figure 7. Coefficient of variation (CV) for each spectral band. (a) to (f) correspond to scenes (a) to (f) of Table 1. The symbols +, square, and triangle mark results of the C, MM, and Gamma method, respectively. Band 6 for TM and ETM+ represents the 6th reflective band at 2.2 μm (also known as Landsat band 7).



A remark concerning TOA reflectance (C method) and surface reflectance (Gamma and MM): the use of TOA reflectance has no adverse effect on the visual appearance. However, as the TOA reflectance in the visible bands usually is higher than the surface reflectance (because of the path radiance contribution) the TOA CV values are lower than the surface reflectance CV values. As the standard deviation for both reflectance products is about the same, the TOA CV values are biased toward lower values. However, this “advantage” is lost if the C method is applied to surface reflectance data. An additional slight advantage of the TOA reflectance for the CV evaluation is the smoothing low pass filter effect of the

atmosphere which yields somewhat smaller standard deviations compared to the surface reflectance product. According to the recommendation of [6] we also investigated the performance of the C method with a smoothed DEM slope map, i.e., using a kernel of 5×5 pixels during the calculation of the slope/aspect maps. However, no improvement was achieved for our scenes. Table 2 shows a summary of all assessments (visual, CV, overall) for all scenes. The overall best rankings are achieved with the MM method.

Table 2. Rankings for all scenes.

<i>Scene ID</i>	<i>Visual Assessment</i>		<i>CV</i>		<i>Overall</i>
	<i>VIS</i>	<i>NIR / SWIR</i>	<i>VIS</i>	<i>NIR / SWIR</i>	
A	MM	MM	C	MM	MM
B	MM	MM	C	MM	MM
C	MM	MM	C	MM	MM
D	MM	MM	C	MM	MM
E	C	MM	C	MM	MM
F	MM	MM	C	MM	MM

4. Conclusions

The performance of three frequently used topographic correction methods was studied for different areas in the Swiss Alps and Israel, using multi-sensor data from SPOT-5, Landsat-5 TM, and Landsat-7 ETM+. The overall best visual ranking is achieved with the modified Minnaert (MM) method, although sometimes the C approach yields better results for the visible bands in the blue to red spectral region. This assessment is generally confirmed by the CV metric, where the C method ranks first for visible bands if the TOA reflectance product is used instead of surface reflectance. This apparent advantage is lost if the C normalization is performed on the surface reflectance product. Although the scope of this study is necessarily limited, it confirms that there is currently no technique with the best ranking in all cases. The problem is aggravated by the fact that the best ranking of methods can even change from one sub-scene to the next one within a larger scene. Further research is needed with imagery on a global basis to derive guidelines on which method performs best under which situation.

Acknowledgements

The authors would like to thank the Swiss Federal Office of Topography (swisstopo) and the Swiss National Point of Contact (NPOC) for providing digital elevation (DHM25) and geocoded SPOT-5 satellite data.

References and Notes

- Justice, C.O.; Wharton, S.W.; Holben, B.N. Application of digital terrain data to quantify and reduce the topographic effect on Landsat data. *Int. J. Remote Sens.* **1981**, *2*, 213–230.

2. Teillet, P.M.; Guindon, B.; Goodenough, D.G. On the slope-aspect correction of multispectral scanner data. *Can. J. Remote Sens.* **1982**, *8*, 84–106.
3. Meyer, P.; Itten, K.I.; Kellenberger, T.; Sandmeier, S.; Sandmeier, R. Radiometric corrections of topographically induced effects on Landsat TM data in an alpine environment. *ISPRS J. Photogramm. Remote Sens.* **1993**, *48*, 17–28.
4. Sandmeier, S.R.; Itten, K.I. A physically-based model to correct atmospheric and illumination effects in optical satellite data of rugged terrain. *IEEE Trans. Geosci. Remote Sens.* **1997**, *35*, 708–717.
5. Richter, R. Correction of satellite imagery over mountainous terrain. *Appl. Opt.* **1998**, *37*, 4004–4015.
6. Riano, D.; Chuvieco, E.; Salas, J.; Aguado, I. Assessment of different topographic corrections in Landsat TM data for mapping vegetation types. *IEEE Trans. Geosci. Remote Sens.* **2003**, *41*, 1056–1061.
7. Shepherd, J.D.; Dymond, J.R. Correcting satellite imagery for the variance of reflectance and illumination with topography. *Int. J. Remote Sens.* **2003**, *24*, 3503–3514.
8. Conese, C.; Gilabert, M.A.; Maselli, F.; Bottai, L. Topographic normalization of TM scenes through the use of an atmospheric correction method and digital terrain models. *Photogramm. Eng. Remote Sens.* **1993**, *59*, 1745–1753.
9. Civco, D.L. Topographic normalization of Landsat Thematic Mapper digital imagery. *Photogramm. Eng. Remote Sens.* **1989**, *55*, 1303–1309.
10. Minnaert, M. The reciprocity principle in lunar photometry. *Astrophys. J.* **1941**, *93*, 403–410.
11. Richter, R. *Atmospheric/Topographic Correction for Satellite Imagery*. Report DLR-IB 565-01/09, **2009**, available online at: <ftp://ftp.dfd.dlr.de/put/richter/ATCOR/>.
12. Dorigo, W. *Retrieving canopy variables by radiative transfer model inversion*. PhD thesis, Technical University of Munich: Munich, Germany. 2008, available online at: <https://www.ipf.tuwien.ac.at/index.php/staff/170-publications-of-wouter-dorigo.html>.

© 2009 by the authors; licensee Molecular Diversity Preservation International, Basel, Switzerland. This article is an open-access article distributed under the terms and conditions of the Creative Commons Attribution license (<http://creativecommons.org/licenses/by/3.0/>).